



# Ultrahigh sensitive gas sensors based on slotted photonic wire-based structures including optical microcavities

Mohammad-Mahdi Babakhani-Fard, Ahmadreza Daraei<sup>a</sup> , Naser Hatefi-Kargan

Department of Physics, Faculty of Science, University of Sistan and Baluchestan, Zahedan, Iran

Received: 22 July 2019 / Accepted: 17 February 2020 / Published online: 27 February 2020  
© Società Italiana di Fisica and Springer-Verlag GmbH Germany, part of Springer Nature 2020

**Abstract** In this paper, we investigated two-dimensional (2D) and three-dimensional (3D) finite element method (FEM) simulations to provide ultrasensitive gas sensors based on silicon-on-insulator (SOI) slotted photonic wire structures in the mid-IR spectral region, tuned for the wavelength  $3.392 \mu\text{m}$ . The proposed optical microstructures have the ability to detect methane gas in the environment in addition to sensing the gas flux from the hole/slot regions with a very high sensitivity ( $S = 2.97$ ) through a very high confinement of the electric field in the photonic wire slot region that leads to an increase in the interaction of light with gas. To further boost the sensitivity of the SOI slotted photonic wire structure to the methane gas, we designed an optical microcavity in the photonic crystal (PhC) slotted structure. This microcavity can sense the smallest methane gas level ( $0.36062 \mu\text{m}^2$ ) with high sensitivity ( $S = 27.45$ ), by means of strengthening the high-quality factor cavity mode and reduction of effective modal volumes. In addition, the ultra-wide bandgap ( $1.9 \mu\text{m}$ ) obtained from Bragg mirrors of the simulated microcavity structures can facilitate us to extend the sensing in a wide range of wavelengths.

## 1 Introduction

Nowadays, optical sensors as high-tech and well-known tools have numerous applications in various fields such as chemistry, medicine, biology, health, safety and laboratory, which requires a very compact, accurate, reliable and albeit cost-effective optical device [1, 2]. Due to the high accuracy and high sensitivity of recognition and detection of chemical products, optical gas sensors have been considered by researchers in the field of chemistry [3]. The presence of toxic and dangerous gases in an environment that endangers human health and even leads to human death, more and more reveals the requirement for the highly sensitive optical sensor for sensing toxic gases [3]. Methane gas is a highly flammable gas which has potential to be combined with other chemicals at very low levels of about 5% and has the risk of explosion [4]. Typically, when methane gas is combined with hydrogen sulfide, it smells unpleasant that might represent a dangerous alarm for a painful explosion. Methane gas, however, itself is not toxic, but when combined with some substances, it has a high potential for toxicity [4]. Methane gas, on the other hand, is one of the most valuable fossil fuels that

<sup>a</sup> e-mail: [daraei@phys.usb.ac.ir](mailto:daraei@phys.usb.ac.ir) (corresponding author)

is naturally extracted from the ground, thus optical methane gas sensor can be identified as a capable explorer to discover methane gas resources that are worth exploiting.

Nowadays, different photonic structures are considered by many optical sensor manufacturers including ridge waveguides, PhC cavities, Mach–Zehnder interferometers, surface plasmon resonators, microring resonators, and fiber Bragg gratings [5–9]. The structure and dielectric elemental parts of these photonic circuits should be capable of fully transmitting light to achieve passive functions such as emission, detection, amplification, and switching [10]. It is clear that only one class of materials cannot fully meet these requirements simultaneously, but it can be assured that silicon photonics, as a key technology, produces ultra-compact photonic integrated circuits (PICs) [10]. The transparency of the SOI waveguides in the telecommunication windows and the high refractive index contrast between silicon and silica in these structures have made it possible to fabricate ultra-compact photonic wires with very low light losses ( $\sim 2$  dB/cm), which provide requirements of many highly sensitive optical sensors [10].

The SOI waveguides are popular photonic wires due to the creation of a light transmission mechanism in a low-refractive-index material (which is requisite of the biochemical liquid and gas sensing) and compatibility with ultra-compact CMOS-manufacturing technology and subsequently have found applications in different fields such as optical sensor, optical polarizer, optical mode converter, mode filtering, and PICs [1, 11–14]. The integrated structures of optical waveguides such as SOI with high-refractive-index contrast, as a robust PIC optical sensor, in addition to supporting sensing modes with very low losses, enable coupling these modes effectively with other optical modes and facilitate sensory operations to a much higher degree of sensitivity [15, 16].

The particular advantage of the SOI slotted photonic wires is the amplification and strong confinement of the electric field in the slot region (low-refractive-index material) which is created in the core (high-refractive-index region) [17]. Such optical structures that are introduced in the references [18] and [19] have found outstanding applications in the field of optical sensors, electro-optic modulators and lasers due to their capability of confining the electric field and trapping the desired optical mode in the slot region [20].

The PhC microcavities with high-quality (Q) factor are able to filter undesired optical modes by means of the photonic band gap (PBG) and to intensify/confine certain optical modes in a cavity with very small effective modal volume ( $V_{\text{eff}}$ ). Thus, the photons lifetime in the cavity can be increased to provide low-threshold nanolasers. They could have a very high Q/V ratio and play a significant role in the cavity quantum electrodynamics studies, minimization of nonlinear optical processing for classical and quantum optical applications and development of the nano-photonic devices, especially optical sensors [21–24]. By increasing the interaction of the electric field of light with the sensing material, these structures are suitable for designing highly sensitive refractive index optical sensors, that deliver sensor operation in a wide range of frequencies by generating the broad bandgap [25, 26].

In this paper, we propose different designs for sensors with high sensitivity based on SOI photonic wires, including slotted strip waveguides, slot-cylinders including a couple of paraxial cylindrical hollows, and arrays of semi-elliptical-shape holes in the slotted 1D PhC system.

## 2 Photonic structures toward sensing

Among sensing approaches, a couple of approaches are used in this article: a) sensing by slotted SOI photonic wires and b) sensing by slotted SOI PhC cavity.

*Sensing by slotted SOI photonic wires* The basis of sensing in photonic wires is the interaction of the electric field of the guided mode of waveguide with the targeted sensing material, and consequently, the variations of the different optical parameters such as the effective refractive index ( $n_{\text{eff}}$ ) for the materials with different densities and concentrations [3]. Normally, the amount of the interaction of optical guided mode with the sensing material is measured by the amount of the evanescent electrical field confinement around the waveguide core (confinement factor) and the evanescent field ratio (EFR) of the power in the cover medium to the total power of the guided mode [4,27]. Homogenous sensing is a great sensing mechanism for detecting changes in the concentration of gas analytes and chemical solutions surrounding the optical waveguide. This mechanism determines the sensitivity of the photonic wires to these analytes through changing the refractive index of the chemical analyte (that is dependent on its concentration), which results in variations in the effective refractive index of the waveguide [3]. One of the finest optical structures for sensing chemical gases is slotted SOI photonic wire. These structures significantly reduce the optical losses that slow down the sensing process, by very high confinement of the electromagnetic field in the slot region of waveguide, in addition to providing a suitable region for the proper interaction of light–matter [28].

The preferred sensitivity measurement mechanism for the slotted photonic structures ( $S_h$ ) presented in this paper is homogenous sensing, and characterization of the quantity of the interaction of light with the target gas defines by the confinement factor in the cover medium ( $\Gamma_c$ ) and in the slot region ( $\Gamma_s$ ) illustrated in the form of Eqs. (1)–(3) [3]:

$$S_h = \frac{\partial n_{\text{eff}}}{\partial n_c} = \frac{2n_c^0}{Z_0 \mathbf{P}} \iint_{\text{medium}} |\mathbf{E}(x, y)|^2 dx dy = \frac{2n_c^0 \Gamma_c}{Z_0 \mathbf{P}} \iint_{\text{total}} |\mathbf{E}(x, y)|^2 dx dy \quad (1)$$

where

$$P = \iint_{\text{total}} [(\mathbf{E} \times \mathbf{H}^* + \mathbf{E}^* \times \mathbf{H}) \cdot \hat{z}] dx dy \quad (2)$$

$$\Gamma_c = \frac{\iint_{\text{medium}} |\mathbf{E}(x, y)|^2 dx dy}{\iint_{\text{total}} |\mathbf{E}(x, y)|^2 dx dy} \quad \& \quad \Gamma_s = \frac{\iint_s |\mathbf{E}(x, y)|^2 dx dy}{\iint_{\text{total}} |\mathbf{E}(x, y)|^2 dx dy} \quad (3)$$

In the above relations,  $n_c^0$  is the unperturbed refractive index value for the cover medium,  $Z$  is the free space impedance,  $\mathbf{E}$  and  $\mathbf{H}$ , are the electric and magnetic field vectors, respectively. The quantity  $P$  is the Poynting vector component along  $\hat{z}$  which represents the direction of the guided mode propagation in the photonic structure. According to Eq. (1) based on the homogenous sensing mechanism, we can see that the increase in the sensitivity of the slotted photonic wire  $S_h$  to the gas analyte requires an increase in the interaction of light with gas, which results in a decrease in the energy flow per unit area in the time unit of the waveguide  $P$  and thus increases of the  $n_{\text{eff}}$  compared to  $n_c^0$

*Sensing by slotted SOI PhC cavity* A PhC cavity mode with high Q factor and small modal volume can play a significant role in increasing the light–matter interactions and can provide the basis for making ultrasensitive sensors [8]. Therefore, by utilizing this photonic structure, we propose a slotted PhC microcavity based on SOI which is capable of detecting smallest methane surface levels, in addition to sensing gas flow through the structure with very high sensitivity. This structure has also led us to the development of sensing operations in a wide range of wavelengths by creating a very wide photonic bandgap.

The mechanism of the proposed sensor is similar to the slotted SOI photonic wire-based sensor in the homogenous sensing, but the method of measuring optical interaction with the

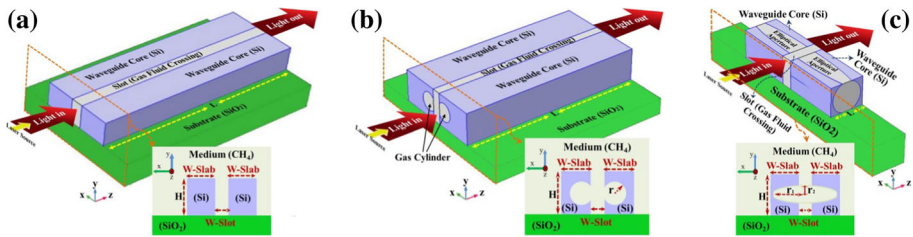


**Fig. 1** Schematic of the optical gas sensor based on SOI **a** slotted strip waveguide, with CH<sub>4</sub> as a cover medium, **b** strip waveguide with Slot-cylinders including (PACHs). **c** Partial unit cell in the structure including arrays of semi-elliptical-shaped holes (ASESH) in the slotted 1D PhC system

target gas is determined by calculating shift of the cavity mode wavelength  $\Delta\lambda_{res}$ . Different deviation of wavelengths,  $\Delta\lambda_{res}$ , related to different levels of methane gas concentrations in the simulations has made it possible to perform detecting and sensing with very high sensitivities by using Eq. (4) [3]:

$$S_h = \frac{\partial\lambda_{res}}{\partial n_c} = \frac{\Delta\lambda_{res}n_g}{\lambda_{res}\Delta n_c} \tag{4}$$

where

$$n_g = n_{eff}(\lambda_{res}) - \lambda_{res} \frac{\partial n_{eff}}{\partial \lambda_{res}} \tag{5}$$

where  $n_g$  is the group refractive index,  $\lambda_{res}$  is the resonant wavelength of the cavity mode, and  $\Delta n_c$  is the change in the refractive index of the gas analyte, that means the cover medium.

### 3 Sensor models based on soi photonic wires

#### 3.1 SOI slotted strip waveguide

From the spectroscopic point of view, the transitions energy spectra for chemical gasses such as CH<sub>4</sub>, H<sub>2</sub>O, CO<sub>2</sub>, CO, NO<sub>2</sub>, NO, and N<sub>2</sub>O are within the spectral range of vibrational, and rotational energy levels in the mid-IR (> 2.5 μm), and they have the absorption and consequently a strong optical interaction in this region [4]. Due to the absorption spectrum peak of methane at the wavelength 3.39 μm, we utilized all of our gas sensor simulations with He–Ne laser ( $\lambda = 3.392 \mu\text{m}$ ) as the source for optical excitation to provide effective light–matter interactions. The basis of the entire optical gas sensor structures in our simulations presented in this paper is the slotted strip waveguide SOI with a silicon substrate and methane gas cover medium; a typical schematic of such structure consists of a silicon core with width W-Slab and height H, which slotted/separated by means of width W-Slot as shown in Fig. 1a.

In fact, this optical structure is used primarily to tune the geometrical parameters for sensing. Thus, the optimized parameters are utilized for the next parts including a couple of para-axial cylindrical hollows (PACHs) (shown in Fig. 1b) and arrays of semi-elliptical-shape holes (ASESH) in the slotted PhC systems (with unit cell depicted in Fig. 1c).

#### 3.2 SOI slot-cylinders and slot-elliptical-holes strip WGs

The dimensions and geometry of the optical waveguide cores play a significant role in determining the optical parameters such as optical field profiles, frequency cutoff, numerical

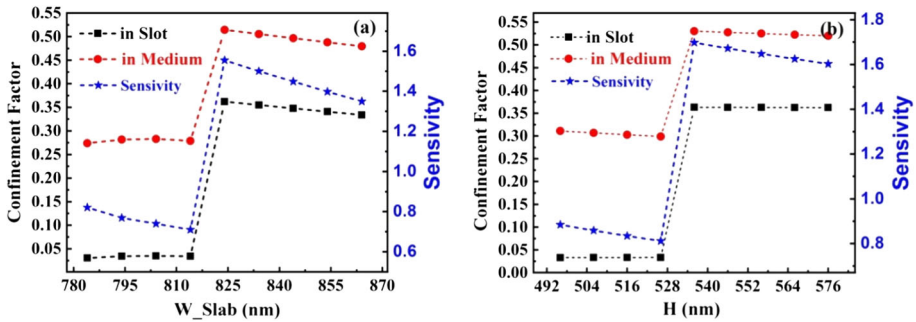


**Fig. 2** Characteristics values of the confinement factor and the sensitivity of gas sensor SOI slotted photonic wire structures. **a** For different widths of silicon core,  $W_{slab}$  (with a constant  $W_{slot} = 100$  nm and  $H = 600$  nm); and **b** for different heights of silicon core,  $H$  (with constant  $W_{slab} = 824$  nm and  $W_{slot} = 100$  nm)

aperture, and optical polarization [29,30]. Therefore, by using two-dimensional (2D) and three-dimensional (3D) FEM simulations and optimizing the dimensions of the silicon core of this photonic wire in order to maximize the confinement factor in the slot and cover medium, this optical structure has been optimized for a gas sensor, as the schematics are shown in Fig. 1b, c. As can be seen in Fig. 1b, a couple of para-axial hollows with circular cross sections (radii  $r$ ) are considered in the core of slotted waveguide that can increase the sensitivity of structure containing methane gas. Also, in another proposed structure, as can be seen in the unit cell of Fig. 1c, semi-elliptical-shaped holes (SESH) are made symmetrically on both sides of the slot with dimensions depicted in the figure. The unit cell has been extended as an array throughout the axis of the slotted PhC waveguide structure.

The refractive index ( $n_c$ ) and the absorption of methane gas ( $\alpha$ ) at wavelength  $3.392 \mu\text{m}$  are  $1.00044$  and  $8.2 \times 10^{-5} \text{ Pa}^{-1} \text{ cm}^{-1}$  ( $8.3 \text{ atm}^{-1} \text{ cm}^{-1}$ ), respectively. The refractive indices of silicon core ( $n_{Si}$ ) and the silica substrate ( $n_{SiO_2}$ ) at wavelength  $3.392 \mu\text{m}$  are  $3.430$  and  $1.411$ , respectively. We used the quasi-TE polarization to provide more effective interaction between light and matter in the structure of gas sensors as it delivers stronger evanescent electric field at the lateral boundaries of the silicon core, while quasi-TM polarization does this at the lower boundary of the waveguide, so penetrates more into the substrate, and reduces the interactions.

## 4 Modeling the gas sensor based on photonic wires

### 4.1 Sensing by SOI slotted strip waveguide

In the first step, by using 2D and 3D FEM simulations, for the preparation of a SOI structure gas sensor which is basis for the other gas sensors proposed in this paper, the core dimensions, slot width, and waveguide length are optimized in order to maximize the confinement factors in the slot and cover medium), and consequently maximize the sensitivity of the structure for methane gas. The results of these optimizations, as shown in Figs. 2 and 3, led to  $W_{slab} = 824$  nm and  $H = 536$  nm for silicon core, and width of slot  $W_{slot} = 100$  nm, and  $L = 3.5 \mu\text{m}$  for the length of the wire.

An example of the field distributions of quasi-TE polarization in the slotted photonic wire structures with optimal dimensions  $W_{slab} = 824$  nm and  $H = 536$  nm for the silicon

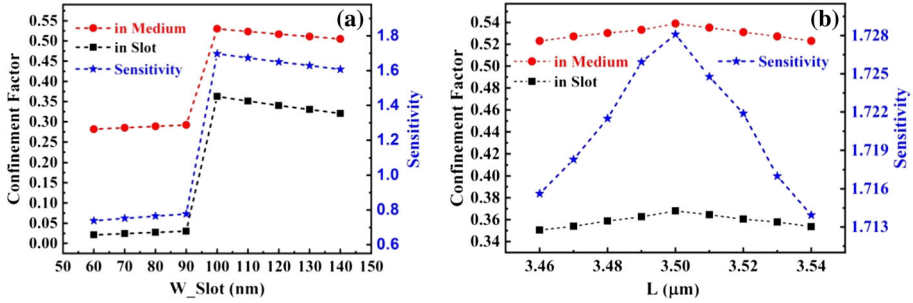


**Fig. 3** Characteristics values of the confinement factor and the sensitivity of gas sensor SOI slotted photonic wire structures. **a** For the various widths of the slot,  $W_{slot}$  (with a constant  $W_{slab} = 824$  nm and  $H = 536$  nm); and **b** for different lengths of photonic wires,  $L$  (with constant  $W_{slab} = 824$  nm,  $H = 536$  nm and  $W_{slot} = 100$  nm)

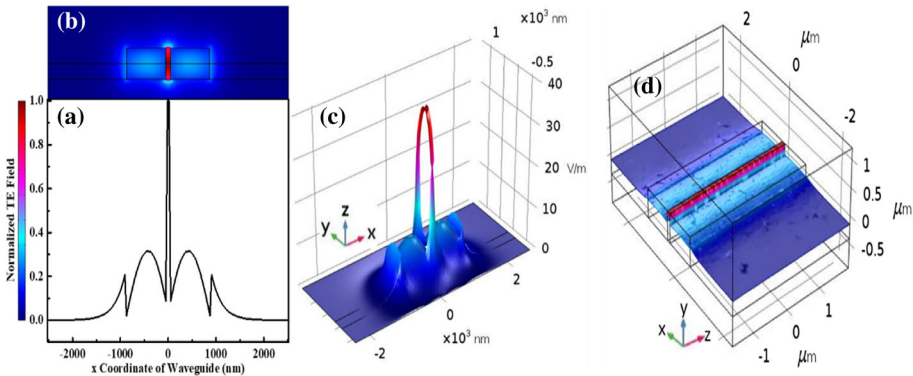


**Fig. 4** The normalized quasi-TE polarization field variation and distribution: **a** variation across waveguide  $x$  coordinate, **b** and **c** 2D and 3D view of field distribution in  $x$ - $y$  cross section, respectively, and **d** the 3D structure of the slotted photonic wire gas sensor with the geometrical parameters:  $W_{slab} = 824$  nm,  $H = 536$  nm,  $W_{Slot} = 100$  nm and  $L = 3.5$  μm

core,  $W_{slot} = 100$  nm, and the length of photonic wires  $L = 3.5$  μm, which results in a maximum sensitivity of  $S \sim 1.72$ , is shown in Fig. 4.

As is evident in the figure, the concentration of the TE field in the slot region is maximized and significant evanescent fields are observed in the waveguide sides.

#### 4.2 Sensing by SOI slot-cylinders strip waveguide

To further enhance the sensitivity of the optimized photonic wire to methane, we included a couple of PACHs which are para-axial cylindrical hollows with a circular cross section containing methane gas, shown in Fig. 1b. The results of the optimization of the hollows radii,  $r$ , in order to maximize the confinement factors in the slot and cover medium region and the sensitivity of slot-cylinders strip waveguide structure, are shown in Fig. 5d. The maximum sensitivity value of  $S \sim 2.50$  is achieved for radii  $r = 195$  nm; the related normalized quasi-TE polarization field variation and distribution in the optimized structure are shown in Fig. 5a-c. The improvement in the sensitivity is attributed to the presence of mixed slot and cylindrical hollows that makes larger effective refractive index variation in the structure.



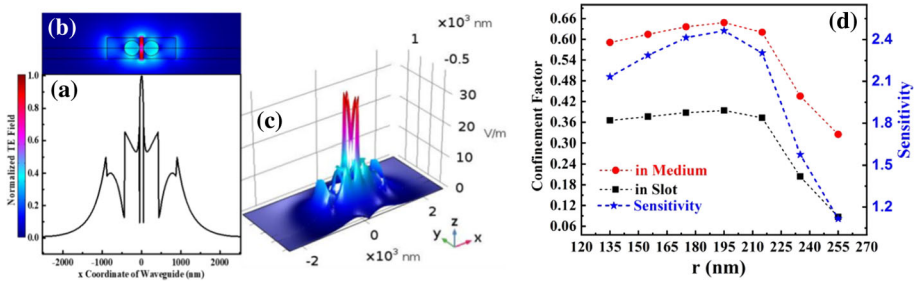


**Fig. 5** **a** The normalized quasi-TE polarization field variation and distribution: **a** variation across waveguide x coordinate, **b** and **c** 2D and 3D view of field distribution in x–y cross section, respectively, related to the slot-cylinders strip waveguide gas sensor with the geometrical parameters:  $W_{\text{slab}} = 824$  nm,  $H = 536$  nm,  $W_{\text{Slot}} = 100$  nm, and  $r = 195$  nm. **d** Confinement factor and sensitivity of the structure for the above dimensions and various radii  $r$  of the cylinders

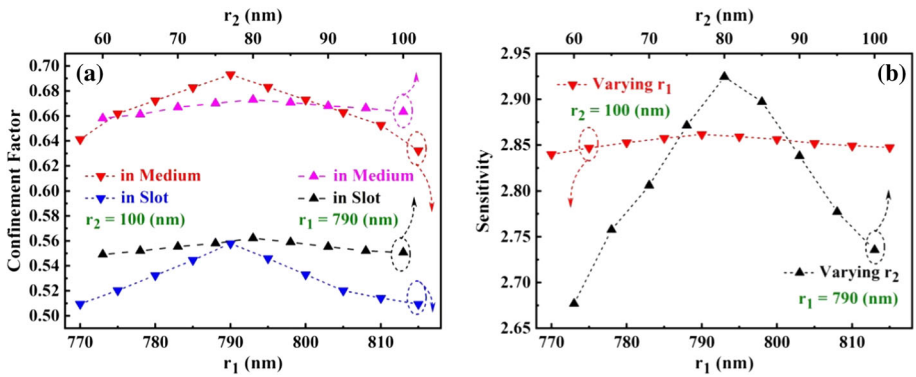


**Fig. 6** Graphs of **a** confinement factor and **b** sensitivity of gas sensor SOI ARESH strip waveguide, for the various  $r_1$  (with a constant  $r_2 = 100$  nm and  $d = 0$  nm), and for the various  $r_2$  (with constant  $r_1 = 790$  nm and  $d = 0$  nm). ( $W_{\text{slab}} = 824$  nm,  $H = 536$  nm and  $W_{\text{slot}} = 100$  nm)

### 4.3 Sensing by SOI ARESH strip waveguide

Another structure that is simulated toward a gas sensing purpose is based on ARESH that is consist of arrays of semi-elliptical-shape holes in the slotted PhC system that the partial unit cell is shown in Fig. 1c. The results of these optimizations in 2D and 3D FEM simulations for different radii  $r_1$  and  $r_2$  (introduced in Fig. 1c), and different distance of ellipsoid long axis to the horizontal reference line ( $y = 0$ ),  $d$ , which are shown in Figs. 6 and 7, indicate that the optimized values are  $r_1 = 790$  nm,  $L = 400$  nm ( $r_2 = 200$  nm) and  $d = -150$  nm. The sensitivity value is  $S \sim 2.97$  which is the best provided in this article so far. Therefore, we chose this structure as the unit cell in designing a Bragg mirror of 1D PhC microcavity that will be presented in the next section.

The distribution of a quasi-TE field in an SOI ARESH strip waveguide sensor structure with optimal dimensions  $r_1 = 790$  nm,  $L = 4 \mu\text{m}$  ( $r_2 = 200$  nm) and  $d = -150$  nm, shown in Fig. 8, confirms the unique ability of this structure to confine optical field in the waveguide slot region.

The SOI-based ARESH in the slotted PhC system proposed in this paper, facilitates the sensing operation for methane gas flux sensing with high sensitivity by preventing the exces-

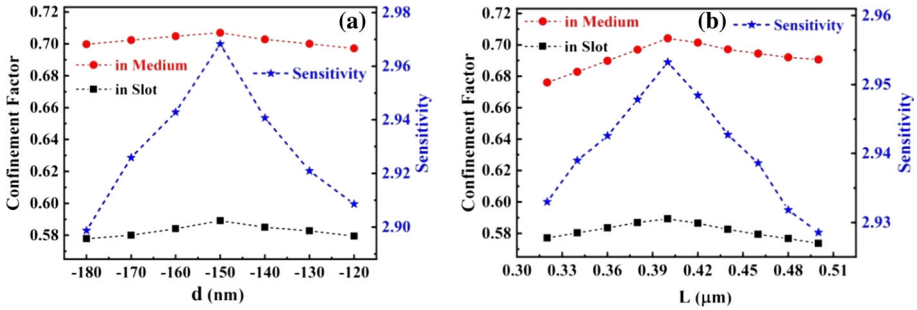


**Fig. 7** Graphs of the confinement factor and the sensitivity of gas sensor SOI ARESH strip waveguide, **a** and **c** for the different distance of ellipsoid long axis to the horizontal reference line ( $y = 0$ ),  $d$ , (with a constant  $r_1 = 790$  nm and  $r_2 = 80$  nm); and **b** and **d** for different lengths of the structure,  $L$  (with constant  $r_1 = 790$  nm and  $d = -150$  nm). ( $W_{\text{slab}} = 824$  nm,  $H = 536$  nm and  $W_{\text{Slot}} = 100$  nm)

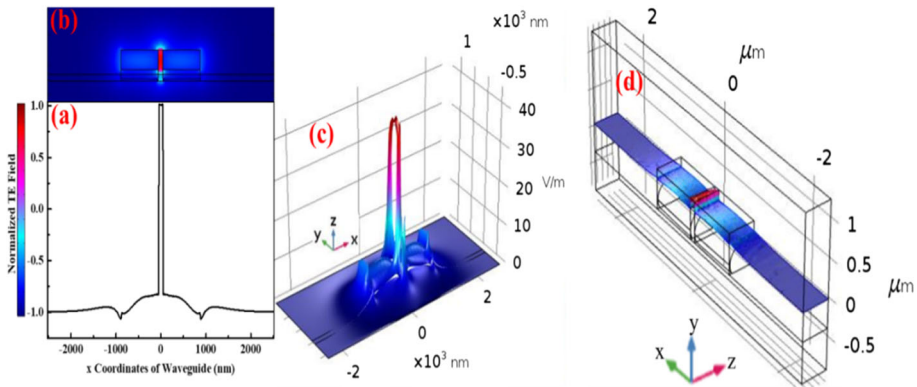


**Fig. 8** The normalized quasi-TE polarization field variation and distribution: **a** variation across waveguide  $x$  coordinate, **b** and **c** 2D and 3D view of field distribution in  $x$ - $y$  cross section, respectively, and **d** the 3D structure of the SOI ARESH strip waveguide, for optimal dimensions  $r_1 = 790$  nm,  $L = 4$   $\mu\text{m}$  ( $r_2 = 200$  nm), and  $d = -150$  nm. ( $W_{\text{slab}} = 824$  nm,  $H = 536$  nm and  $W_{\text{Slot}} = 100$  nm)

sive penetration of modes beyond neighboring regions of waveguide (which are found in sensors based on conventional strip and rib waveguides) and concentrating it in the region of the slotted PhC structure, in addition to reducing optical losses in the waveguide.

### 5 Modeling gas sensor based on PhC microcavity

#### 5.1 PhC microcavity design

The unique ability of PhC cavities to confine and intensify optical modes with a high Q factor and a small modal volume provides motivations for designing a slotted PhC microcavity-based structure for methane gas sensing. For this purpose, the structure ARESH discussed in the previous section was used as Bragg mirrors. The schematic of such optimized Bragg mirror design consisting 11 pairs of semi-elliptical-shaped holes (with  $r_1 = 790$  nm and  $r_2 = 200$  nm) with a period constant of  $a = 704.225$  nm in the silicon core including slot along the  $z$  (with optimal dimensions  $W_{\text{slab}} = 824$  nm and  $W_{\text{Slot}} = 100$  nm) is shown



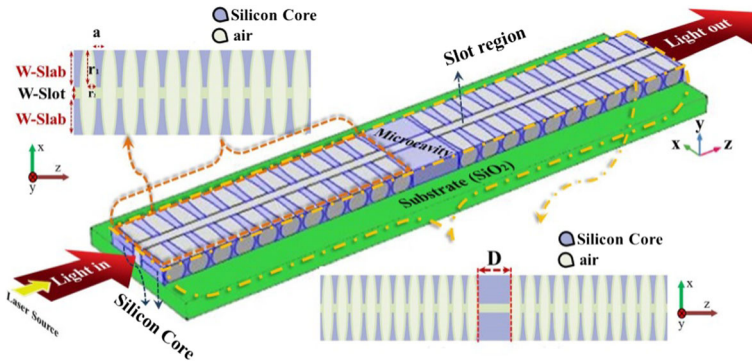


**Fig. 9** Schematic of ARESH as Bragg mirror (top-left corner), and 1D PhC Fabry-Pérot microcavity design, with cavity length  $D$

in the upper-left corner in Fig. 9. The designed PhC Bragg mirrors that sandwich the cavity, offer a very large bandgap (about  $1.9 \mu\text{m}$ ) around the center wavelength of  $3.39 \mu\text{m}$ , as shown in Fig. 10a that causes sensor functionality in a wide range of wavelengths.

The microcavity is defined as a Fabry-Pérot cavity with a length of a lambda, as the schematic is shown in Fig. 9, consisting of two ARESH type Bragg mirrors modeled in the  $z$ -direction. The results of our 2D FEM simulation (Fig. 10b) show that for the cavity with a length  $3.392 \mu\text{m}$  ( $\lambda$  cavity) fundamental TE mode has a high-enough Q factor of 110 and a small effective volume of  $V_{\text{eff}} = 1.8 (\mu\text{m})^3$ , that is capable of detecting very small levels of methane gas with an extremely high sensitivity of  $S \sim 27.45$ , which has improved more than nine times better than normal ARESH sensor structure.

To tune the ARESH system as Bragg mirror and the  $\lambda$ -Cavity in our 1D PhC structure for the resonance wavelength  $\lambda_{\text{res}} = 3.392 \mu\text{m}$  with a high Q factor and a small effective modal volume  $V_{\text{eff}}$ , the following equations were used:

$$2r_2 = \frac{\lambda_{\text{res}}}{4n_{\text{air}}} \quad \& \quad a = \frac{\lambda_{\text{res}}}{4n_{\text{Si}}} \quad \& \quad D = \frac{m\lambda_{\text{res}}}{2n_{\text{Si}}} \tag{6}$$

where

$$Q = \frac{\lambda_{\text{res}}}{\Delta\lambda_{\text{FWHM}}} \quad \& \quad V_{\text{eff}} = \frac{\left( \int_V \varepsilon(\vec{r}) |\vec{E}(\vec{r})|^2 d^3\vec{r} \right)}{\max(\varepsilon(\vec{r}) |\vec{E}(\vec{r})|^2)} \tag{7}$$

The optimized radius  $r_2$  that is introduced in Fig. 1c is  $r_2 = 200 \text{ nm}$ ,  $n_{\text{air}}$  is the refractive index of the air,  $n_{\text{Si}}$  is the silicon core refractive index ( $n_{\text{Si}} = 3.43$ ),  $m$  is an integer ( $m = 2$ ),  $\Delta\lambda_{\text{FWHM}}$  is the cavity mode's width,  $\varepsilon(\mathbf{r})$ , the dielectric constant of the silicon core and  $\mathbf{E}(\mathbf{r})$  is the electric field of the cavity mode. Our calculations and optimizations of the transmission and reflection spectra by the 2D FEM method, for a cavity length of  $D = 0.988 \mu\text{m}$  and 11 pairs in the Bragg mirrors with a periodic constant of  $a = 704.225 \text{ nm}$  for the fundamental mode with a wavelength of  $3.392 \mu\text{m}$  in the structure, are illustrated in Fig. 10c–e, assure very high capability of microcavity provided for the sensing wavelength of  $3.392 \mu\text{m}$  (methane gas absorption peak).

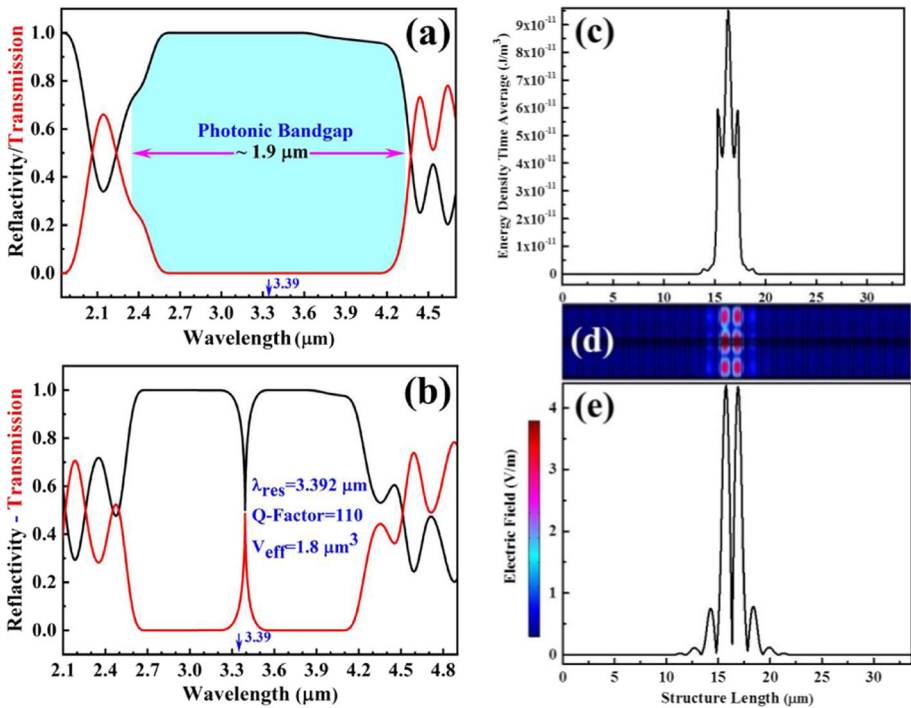


**Fig. 10** Reflectivity and transmission spectra in the proposed 1D PhC structures **a** for the Bragg mirrors, **b** microcavity design in the wavelength range 2.1–4.9 μm; **c** the average energy density of the mode; **d** and **e** the electric field mode map and distribution

### 5.2 Sensing by 1D PhC microcavity

Based on the structure introduced in the previous section, with the tuned cavity wavelength of  $\lambda_{res} = 3.392 \mu\text{m}$ , we examined the proposed structure for detecting and sensing methane gas with different gas analyte densities. Due to the optical cavity mode with gas material interactions, the mode’s wavelength shifts with different amount depends on the different gas densities. To illustrate the sensitivity of this structure to the various methane gas densities, we consider proximate regions as a gas chamber with a length of  $D \approx 0.988 \mu\text{m}$  ( $\approx$  equal to the cavity length) and thickness of  $g$  which make a gas chamber region, as the schematic is shown in Fig. 11. By calculating the cavity wavelength mode shift ( $\Delta\lambda_{res}$ ) and the optical field confinement factor in the gas chamber region in terms of different  $g$  thickness for gas flow region (with  $W_{Slot}$  and length  $D$  as constants and parameter “ $g$ ” as a variable), we attained the sensitivity of the microcavity structure and all the relevant results are depicted in Fig. 12a, b and their insets. A significant shift of the resonant wavelength of the microcavity mode  $\Delta\lambda_{res} = 12.23 \text{ nm}$  at a resonant wavelength  $\lambda_{res} = 3.392 \mu\text{m}$  due to the strong interaction of the optical field of the microcavity structure with a very small methane gas level of  $0.36062 \mu\text{m}^2$  (for  $g = 365 \text{ nm}$ ), depicted in the inset of Fig. 12b, shows the ability of this 1D PhC microcavity design to detect and sense even the smallest gas densities, with a high amount of sensitivity  $S \sim 27.45$ .

Finally, to examine the performance of the structure for sensing in terms of the concentration of methane gas, we exposed the system to the flow of surrounded gas especially around the

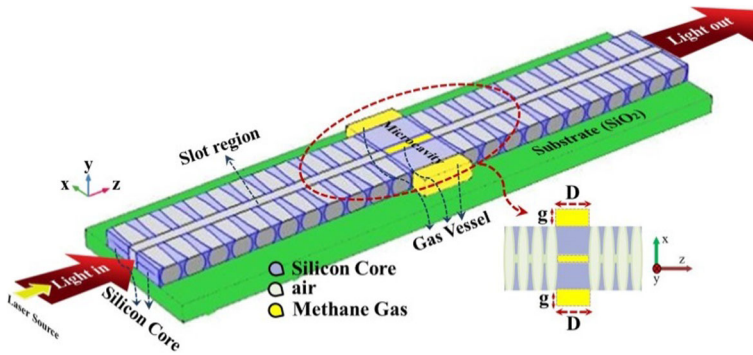


**Fig. 11** Schematic of the gas chamber with a length of  $D \approx 0.988 \mu\text{m}$  ( $\approx$  equal to the cavity length)  $W_{\text{Slot}} = 100 \text{ nm}$  and thickness of  $g$  in the 1D PhC microcavity sensor

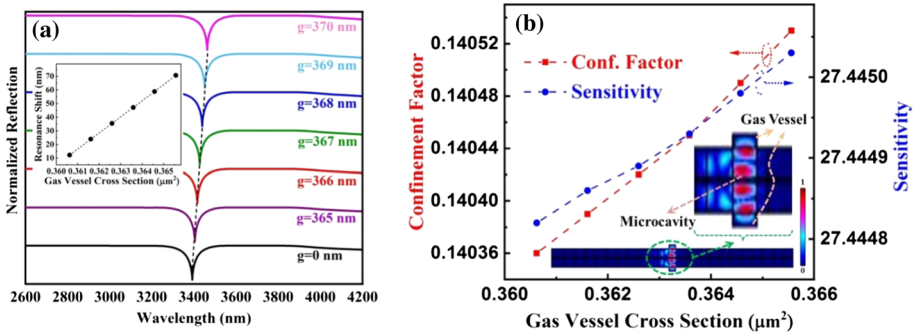


**Fig. 12** **a** The reflection spectra of the microcavity sensor; inset: corresponding shift of the resonant wavelength; **b** the optical field confinement factor in the gas chamber region and sensitivity of the designed sensor structure for different levels of methane gas; inset: The interactions of the TE mode with methane gas in the region with cross-sectional area  $0.36062 \mu\text{m}^2$  (for a width  $g = 365 \text{ nm}$ )

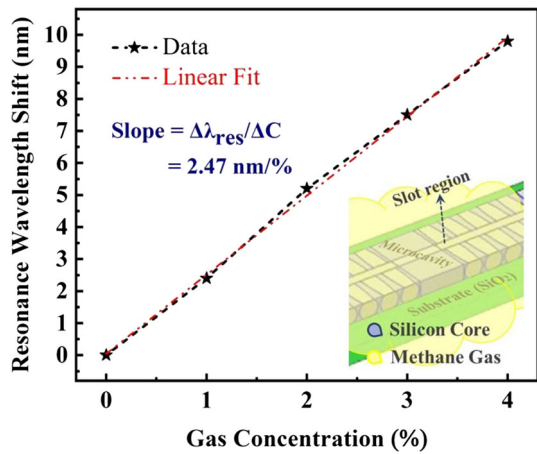
slotted cavity, as depicted in the inset of Fig. 13. The shift in the cavity resonance wavelength of the mode as a function of increased methane gas concentration in simulation is calculated via linear fit to the data. The result for the sensitivity was  $S = \Delta\lambda_{\text{res}}/\Delta C = 2.47 \text{ nm}/\%$  which corresponds to  $S = \Delta\lambda_{\text{res}}/\Delta n \approx 404 \text{ nm}/\text{RIU}$

Since the molecules containing the C–H bond have an intense absorption and interaction in the spectral region 3.0–3.7  $\mu\text{m}$ , and the sensor wavelengths of all the gas sensor structures presented in this paper are around  $\lambda \approx 3.392 \mu\text{m}$  is the methane gas absorption peak, the proposed gas sensors here can be generalized to other analytes that have the CH bond.

### 6 Conclusions

In this paper, through 2D and 3D FEM simulations, we presented three highly sensitive sensors based on SOI photonic wires, including slotted strip waveguides, slot-cylinders including (PACHs), and arrays of semi-elliptical-shaped holes (ASESH) in the slotted 1D PhC system. These structures are characterized by operating He-Ne laser ( $\lambda = 3.392 \mu\text{m}$ ) as the source for optical excitation (at methane gas absorption spectrum peak). By means of strong confinement control of the quasi-TE modes in the slot region of waveguides in addition to reducing

**Fig. 13** The resonance wavelength shift of the cavity mode as a function of increased methane gas concentration; inset: schematic of the structure showing gas flow region



optical losses in the slotted waveguides, very high sensitivity obtained for the three structures  $S \approx 1.72, 2.50, 2.97$ , respectively, enables detecting methane gas in the environment in addition to sensing the gas flux from the hole/slot regions. Subsequently, we simulate a 1D PhC microcavity sensor structure based on ARESH as mirrors to enhanced TE mode and increase the interaction of the optical field with the target gas. The structure can achieve the ability to sense the smallest methane gas level,  $0.36062 \mu\text{m}^2$  with high sensitivity,  $S = 27.45$ , that is nearly one order of magnitude improvement in comparison with the normal ARESH sensor structure. Besides, through Bragg mirrors of such simulated microcavity structures, the ultra-wide bandgap ( $1.9 \mu\text{m}$ ) can be created to facilitate a system for spreading out the sensing in a wide range of wavelengths. Moreover, since the transitions energy spectra for chemical gasses, such as  $\text{CH}_4, \text{H}_2\text{O}, \text{CO}_2, \text{CO}, \text{NO}_2, \text{NO}$ , and  $\text{N}_2\text{O}$  are within the spectral range of vibrational and rotational energy levels in the mid-IR ( $> 2.5 \mu\text{m}$ ), and also molecules containing the C–H bond have an intense absorption and accordingly a strong optical interaction in the spectral region  $3.0\text{--}3.7 \mu\text{m}$ , all the designed gas sensors in this paper can be generalized to analytes for sensing these gases.

## References

1. S. Ghosh, T. Dar, C. Vipavakit, C. Pan, N. Kejalakshmy, B. Rahman, Compact photonic SOI sensors, in *Computational Photonic Sensors*, ed. by M. Hameed, S. Obayya (Springer, Cham, 2019), pp. 343–383
2. K. Yamada, Silicon photonic wire waveguides: fundamentals and applications, in *Silicon Photonics II. Topics in Applied Physics*, vol. 119, ed. by D. Lockwood, L. Pavesi (Springer, Berlin, 2011), pp. 1–29
3. M. La Notte, B. Troia, T. Muciaccia, C. Campanella, F. De Leonardis, V. Passaro, Recent advances in gas and chemical detection by Vernier effect-based photonic sensors. *Sensors* **14**(3), 4831–4855 (2014)
4. M. Butt, S. Degtyarev, S. Khonina, N. Kazanskiy, An evanescent field absorption gas sensor at mid-IR  $3.39 \mu\text{m}$  wavelength. *J. Modern Opt.* **64**(18), 1892–1897 (2017)
5. J.G. Wangüemert-Pérez, A. Hadij-ElHouati, A. Sánchez-Postigo, J. Leuermann, D.-X. Xu, P. Cheben, A. Ortega-Moñux, R. Halir, Í. Molina-Fernández, Subwavelength structures for silicon photonics biosensing. *Opt. Laser Technol.* **109**, 437–448 (2019)
6. C.-S. Deng, M.-J. Li, J. Peng, W.-L. Liu, J.-X.B. Zhong, Simultaneously high-Q and high-sensitivity slotted photonic crystal nanofiber cavity for complex refractive index sensing. *JOSA B* **34**(8), 1624–1631 (2017)
7. H.K. Hisham, Fiber Bragg Grating, *Sensors: Development and Applications: Development and Applications* (Taylor & Francis Group, Routledge, 2019)

8. C. Consani, C. Ranacher, A. Tortschanoff, T. Grille, P. Irsigler, B. Jakoby, Mid-infrared photonic gas sensing using a silicon waveguide and an integrated emitter. *Sens. Actuators B Chem.* **274**, 60–65 (2018)
9. M. Butt, S. Khonina, N. Kazanskiy, Plasmonic refractive index sensor based on metal-insulator-metal waveguides with high sensitivity. *J. Modern Opt.* **66**(9), 1038–1043 (2019)
10. Y. Halioua, A. Bazin, P. Monnier, T. Karle, G. Roelkens, I. Sagnes, R. Raj, F. Raineri, Hybrid III–V semiconductor/silicon nanolaser. *Opt. Express* **19**(10), 9221–9231 (2011)
11. M.F.O. Hameed, A.S. Saadeldin, E.M. Elkaramany, S. Obayya (eds.), *Silicon nanowires for DNA sensing, Computational Photonic Sensors* (Springer, New York, 2019), pp. 321–342
12. X. Wang, J. Dong, Ultrashort polarization rotator based on cross-symmetry waveguide. *Opt. Commun.* **367**, 68–71 (2016)
13. D. Dai, Y. Tang, J.E. Bowers, Mode conversion in tapered submicron silicon ridge optical waveguides. *Opt. Express* **20**(12), 13425–13439 (2012)
14. M. Sieger, B. Mizaikoff, Optimizing the design of GaAs/AlGaAs thin-film waveguides for integrated mid-infrared sensors. *Photon. Res.* **4**(3), 106–110 (2016)
15. Q. Deng, Q. Yan, L. Liu, X. Li, J. Michel, Z. Zhou, Robust polarization-insensitive strip-slot waveguide mode converter based on symmetric multimode interference. *Opt. Express* **24**(7), 7347–7355 (2016)
16. T. Komljenovic, M. Davenport, J. Hulme, A.Y. Liu, C.T. Santis, A. Spott, S. Srinivasan, E.J. Stanton, C. Zhang, J.E. Bowers, Heterogeneous silicon photonic integrated circuits. *J. Lightw. Technol.* **34**(1), 20–35 (2016)
17. F. Dell’Olio, V.M. Passaro, Optical sensing by optimized silicon slot waveguides. *Opt. Express* **15**(8), 4977–4993 (2007)
18. V.R. Almeida, Q. Xu, C.A. Barrios, M. Lipson, Guiding and confining light in void nanostructure. *Opt. Lett.* **29**(11), 1209–1211 (2004)
19. Q. Xu, V.R. Almeida, R.R. Panepucci, M. Lipson, Experimental demonstration of guiding and confining light in nanometer-size low-refractive-index material. *Opt. Lett.* **29**(14), 1626–1628 (2004)
20. N. Eti, H. Kurt, Model analysis of ridge and rib types of silicon waveguides with void compositions. *IEEE J. Quantum Electron.* **52**(10), 1–7 (2016)
21. Y. Zhang, I. Bulu, W.-M. Tam, B. Levitt, J. Shah, T. Botto, M. Loncar, High-Q/V air-mode photonic crystal cavities at microwave frequencies. *Opt. Express* **19**(10), 9371–9377 (2011)
22. P. Xu, Y. Shi, High Q/V hybrid plasmonic photonic crystal nanobeam cavity: towards low threshold nanolasers application. *Opt. Commun.* **311**, 234–238 (2013)
23. T.-W. Lu, P.-T. Lin, P.-T. Lee, Photonic crystal horizontally slotted nanobeam cavity for silicon-based nanolasers. *Opt. Lett.* **37**(4), 569–571 (2012)
24. M. Banaee, A. Pattantyus-Abraham, M. McCutcheon, G. Rieger, J.F. Young, Efficient coupling of photonic crystal microcavity modes to a ridge waveguide. *Appl. Phys. Lett.* **90**(19), 193106 (2007)
25. A. Daraei, M.E. Daraei, Compact nanocavity with elliptical slot inside photonic wire bandgap materials including sidewalls gratings for biosensing. *Appl. Phys. A* **122**(7), 662 (2016)
26. Y. Yu, T.-H. Xiao, H.-L. Guo, Z.-Y. Li, Sensing of microparticles based on a broadband ultrasmall microcavity in a freely suspended microfiber. *Photon. Res.* **5**(3), 143–150 (2017)
27. P. Bettotti, A. Pitanti, E. Rigo, F. De Leonardis, V. Passaro, L. Pavesi, Modeling of slot waveguide sensors based on polymeric materials. *Sensors* **11**(8), 7327–7340 (2011)
28. H. Zengzhi, Y. Zhang, C. Zeng, D. Li, M.S. Nisar, J. Yu, J. Xia, High confinement factor ridge slot waveguide for optical sensing. *IEEE Photon. Technol. Lett.* **27**(22), 2395–2398 (2015)
29. B.E. Saleh, M.C. Teich, *Fundamentals of Photonics*, 2nd edn. (Wiley, New York, 2007)
30. J.D. Joannopoulos, S.G. Johnson, J.N. Winn, R.D. Meade, *Photonic Crystals: Molding the Flow of Light*, 2nd edn. (Princeton University Press, Princeton, 2008)